Atmos. Meas. Tech. Discuss., 6, 2793–2828, 2013
www.atmos-meas-tech-discuss.net/6/2793/2013/
doi:10.5194/amtd-6-2793-2013

Atmospheric Measurement Techniques Discussions
Open Access

Remote sensing of volcanic ash plumes from thermal infrared: a case study analysis from SEVIRI, MODIS and IASI instruments

P. Dubuisson[1], H. Herbin[1], F. Minvielle[1], M. Compiègne[1], F. Thieuleux[1], F. Parol[1], and J. Pelon[2]

[1]LOA, UMR8518, CNRS, Université Lille 1, Villeneuve d'Ascq, France
[2]LATMOS, UMR8190, CNRS, Université Pierre et Marie Curie, Paris, France

Received: 14 February 2013 – Accepted: 8 March 2013 – Published: 20 March 2013

Correspondence to: P. Dubuisson (philippe.dubuisson@univ-lille1.fr)

Published by Copernicus Publications on behalf of the European Geosciences Union.

Abstract

The Eyjafjallajökull eruption during May 2010 is used as a case study to evaluate the consistency of retrievals from different thermal infrared instruments for the detection and characterization of volcanic ash plumes. In this study, the split window technique is used to estimate the optical thickness, the effective particle size and the mass concentration of volcanic particles from brightness temperatures measured in the infrared atmospheric window (8–12 µm). Retrievals are obtained for several mineral compositions whose optical properties are computed using Mie theory accounting for spectral variations of the refractive index. The method is applied similarly to data from MODIS, SEVIRI and IASI space-borne instruments, using two channels at 11 µm and 12 µm. Despite different instrumental characteristics, the results are in good agreement, which denotes the robustness of the retrieval method and the consistency of the observations. Nevertheless, the refractive index data and altitude used for the plume in the inversion may lead to large uncertainties in retrieved effective size and mass concentration in dense plumes and makes it difficult to estimate its composition. While it brings additional constrains, the use of a third channel (8.7 µm) does not allow determining the nature of the particles. As confirmed with high spectral resolution radiative transfer simulations, hyperspectral sensors, such as IASI, are well-suited to study the particle composition of volcanic plumes.

1 Introduction

Volcanoes are important sources of aerosol particles and gas phase precursors of secondary air pollutants that can have noticeable effects on solar and infrared atmospheric radiation, with consequences on atmospheric radiative forcing and climate (Le Treut et al., 2007). In addition, large plumes of ash emitted in the atmosphere can have consequences on the aviation security and air traffic (Prata and Tupper, 2009). In this context, satellite instruments provide efficient tools for a spatio-temporal monitoring of

AMTD
6, 2793–2828, 2013

ash plumes (Zehner, 2010). This kind of information is very useful for aviation security agencies in order to avoid engine hazards, in complement to in situ measurements as well as numerical simulations. As an example, the explosive eruption of the Eyjafjallajökull volcano in Iceland during April–May 2010 has shown the importance of combining measurements and models to derive physical characteristics of volcanic aerosols and to study the plume spatial structure and dispersion (Zehner, 2010).

Various methodologies have been proposed for plume observations and characterization from active remote sensing technology (Winker et al., 2012) or using passive sensors from space (Prata, 1989a, b). The analysis of spectral information gives access to optical and physical properties of volcanic ash plumes from which parameters in term of flight safety can be derived (e.g. the mass concentration of particles). Especially the split window technique is extensively used to characterize semitransparent clouds using channels in the infrared atmospheric window (8–13 µm), centred approximately at 11 µm and 12 µm (Inoue, 1985, 1987; Parol et al., 1991; Dubuisson et al., 2008). This technique has been also successfully used for the characterization of volcanic particles (Wen and Rose, 1994; Schneider et al., 1995; Prata and Grant, 2001) and it is based on the fact that extinction efficiencies of particles vary with the wavelength in the infrared window. As an example, multi-spectral imaging with sensors onboard geostationary platforms, such as the Meteosat Second Generation (MSG) satellite, is commonly used for an efficient spatio-temporal monitoring of volcanic plumes (Prata and Kerkmann, 2007; Francis et al., 2012; Prata and Prata, 2012).

In this paper, an analysis of the results obtained by applying a common retrieval method to the same volcano plume is presented using observations from MODIS, SEVIRI and IASI space-borne instruments. Indeed, these sensors have adequate spectral characteristics in the infrared spectral region to retrieve optical and physical properties of particles contained in volcanic ash clouds. The retrieval method is based on the split window technique and accurate radiative transfer calculations. The goal is not to present a new operational algorithm, but to study the consistency of retrievals from different infrared instruments and to analyse the uncertainties and limits

AMTD
6, 2793–2828, 2013

of these retrievals. We focus on the eruption of the Eyjafjallajökull volcano in Iceland, on 6 May 2010 because it is very well documented in the literature (thanks to many in situ measurements) and it has been observed near-simultaneously by different space infrared sensors (Zehner, 2010).

MODIS, SEVIRI and IASI instruments are briefly described in Sect. 2. The retrieval algorithm is presented in Sect. 3. Retrievals of particle effective size and mass loading of the plume from two infrared channels are presented and analysed in Sect. 4 using SEVIRI observations in spectral bands at 11 and 12 µm. In this section, contribution of the spectral channel at 8.7 µm to retrievals is also analysed. The methodology is then performed similarly to the considered infrared sensors to assess the consistency of instruments and the spatial distributions of retrieved parameters are compared in Sect. 5. The influence of parameters such as particle type or plume altitude on retrievals is analyzed in Sect. 6 to assess their limit. Finally, we discuss the potential of high spectral resolution interferometer sounders for the retrieval of the plume composition.

2 Description of the instruments

Many space-borne narrow band sensors with adequate spectral response in the infrared window are available to monitor volcanic plumes. These sensors are generally designed to collect aerosol properties at a global scale. More recently, hyperspectral sensors such as IASI (Schlüssel et al., 2005; Clerbaux et al., 2009) or GOSAT (Kuze et al., 2009) have been operated which provide useful information for aerosol characterization from measurements of infrared extinction spectra. In our study, three instruments have been considered:

– SEVIRI on-board the geostationary Meteosat Second Generation (MSG) satellite (Schmetz et al., 2002). Among the available channels, three are centred in the infrared window at 8.7, 10.8 and 12 µm. Data are collected every 15 min for the whole 70 degree disk, with a spatial resolution ranging from $3 \times 3\,km^2$ at the sub-satellite to about $10 \times 10\,km^2$ near the edges of the scan.

AMTD
6, 2793–2828, 2013

– MODIS (Moderate Resolution Imaging Spectroradiometer) on-board the two polar orbiting satellites AQUA and TERRA. This instrument acquires data in 36 channels with three channels in the infrared window (8.6, 11 and 12 µm) at $1 \times 1\,km^2$ spatial resolution, with a viewing swath width of 2330 km and it is designed to retrieve aerosols properties (Remer et al., 2005).

– IASI (Infrared Atmospheric Sounding Interferometer). IASI is a payload element of the MetOp satellites using an accurately calibrated Fourier Transform Spectrometer operating in the 3.7–15.5 µm spectral range, with an apodized spectral resolution of $0.5\,cm^{-1}$ and, consequently, includes the infrared window. This instrument analyses an atmospheric cell of about $50 \times 50\,km^2$ with circular IFOV of 3.33°, which corresponds to a ground resolution of 12 km at nadir (Clerbaux et al., 2009).

Note that due to orbit characteristics of the satellites, it is possible to compare near-simultaneously retrievals from MODIS and SEVIRI.

3 Retrieval methodology

A simple algorithm based on the split window technique has been developed to retrieve optical and physical properties of volcanic plumes from infrared satellite data and using accurate radiative transfer calculations. Note that the goal of this study is not to present an operational algorithm but to provide an efficient methodology to retrieve plume properties from satellite data, using realistic spectral variations of the refractive indices of several volcanic particle types. As mentioned in the introduction, the use of two channels in the thermal infrared allows characterizing volcanic plumes as well as discriminating cloud contamination. As an example, Fig. 1 presents IASI spectra simulated using the radiative transfer code LBLDOM (Dubuisson et al., 2005), based on a line-by-line model coupled to DISORT and adapted to the spectral response of IASI (Herbin et al., 2012). Simulations of brightness temperature are presented for a

AMTD
6, 2793–2828, 2013

clear atmosphere, a volcanic ash plume or an ice cloud at 6 and 10 km height, respectively. The brightness temperatures simulated for SEVIRI are also reported in the figure with the spectral width associated to each channel. We clearly see that the brightness temperatures simulated for the ash plume and the ice cloud are sufficiently different from those obtained for a clear atmosphere to allow pixel identification. In addition, the different slopes between ash plume and ice cloud spectra (especially in the 10 to 12 µm spectral range) makes it possible to discriminate between cloud layers and volcanic plumes. A plume characterization is then possible using Brightness Temperature Differences (BTD) from the split window technique. In the following we describe the radiative transfer modelling and the retrieval methods used for this study.

3.1 Radiative transfer modelling

Brightness temperatures are simulated using the radiative transfer code FASDOM (Dubuisson et al., 2005). This code was originally developed for the IIR/CALIPSO radiometer and has been adapted to MODIS and SEVIRI sensors (Borde et al., 2010). Infrared radiances are calculated by solving the radiative transfer equation in the case of a vertically inhomogeneous plane-parallel atmosphere using the radiative transfer code DISORT developed by Stamnes et al. (1988). Gaseous absorption is considered on the basis of the correlated k distribution method (Lacis et Oinas, 1991), following Kratz (1995). This approach allows accounting for interactions between absorption and scattering processes in presence of cloud and/or aerosol layers. Conversion tables of brightness temperature to radiance, as well as gaseous absorption have been calculated using the true spectral response of the sensors. For calculations, FASDOM requires the thermodynamic profile as well as single scattering properties of particles as an a priori. Note that in the special case of IASI, channels without gaseous absorption at about 8.7, 11 and 12 µm have been selected, in order to facilitate the retrieval process. We use only three channels among the 8431 available IASI channels, in order to perform comparisons for retrievals obtained with the same procedure as for the other instruments.

AMTD
6, 2793–2828, 2013

Optical properties of liquid clouds and aerosols are calculated from the Mie theory assuming spherical particles. This assumption is reasonable in the thermal infrared spectrum (Mehta et al., 2009) in contrast to the solar spectrum for which the particle shape has a non-negligible influence on the top of atmosphere radiances. Several models (i.e. spectral refractive index and size distribution) are considered for volcanic particles. Table 1 presents the particle types used for this study, as well as references used for refractive indices. From these data, single scattering properties of particles (extinction coefficient, single scattering albedo and asymmetry factor) are computed assuming a lognormal formulation for the particle size distribution:

$$n(r) = \frac{N_0}{r \mathrm{Ln}\sigma\sqrt{2\pi}} \exp\left(-\frac{1}{2}\frac{\left[\mathrm{Ln}r - \mathrm{Ln}r_0\right]^2}{\left[\mathrm{Ln}\sigma\right]^2}\right), \quad (1)$$

where N_0 is the total number density, r is the particle radius, r_0 is the geometric mean radius. In addition, σ is the geometric standard deviation of the particle size distribution and it is fixed to 2 in this study, because this value is within the range of volcanic particles typically measured (Hess et al., 1998; Dubovik et al., 2002). From this formulation, the effective radius r_e can be defined as:

$$r_e = \frac{\int_0^\infty r^3 n(r)\mathrm{d}r}{\int_0^\infty r^2 n(r)\mathrm{d}r}. \quad (2)$$

The split window technique is based on the spectral variation of the particles extinction that can be measured by comparing two thermal infrared channels. In order to get a good accuracy, we compute the single scattering optical properties with a high spectral resolution (1 cm^{-1}) and then integrated over the real spectral response of each channel. Practically, Look-Up-Tables (LUTs) of these integrated properties have been built

AMTD
6, 2793–2828, 2013

for each spectral channel and for each particle type with effective radius varying from 0.5 to 20 µm with a grid step of 0.25 µm.

As an example, Fig. 2 presents BTD obtained from radiative transfer calculations for SEVIRI channels at 11 µm and 12 µm. These simulations are performed with various optical thicknesses and effective particle sizes for three particle types corresponding to volcanic aerosols (andesite), liquid clouds and ice clouds. For a given particle type, Fig. 2 illustrates that a simultaneous estimate of the optical thickness and effective size is possible from a pair of brightness temperatures, at least in theory, as well as cloud discrimination. Indeed, BTD obtained for the volcanic plume are of opposite as those found for clouds. However, Fig. 2 also shows that only small volcanic particles can be detected, corresponding to a maximal effective radius of 8 µm in this case. Simulations (not illustrated here) have shown that the maximal effective radius that can be detected varies depending on the particle type. As an application, Fig. 3 presents BTD observed for the Eyjafjallajökull eruption during May 2010, from MODIS infrared channels at 11 µm and 12 µm. This confirms the different spectral behaviour of cloud and volcanic particles already presented in Fig. 2.

3.2 Retrieval algorithm description

The retrieval algorithm has been developed following the scheme proposed by Dubuisson et al. (2008). This algorithm was originally developed for cirrus clouds and has been adapted in order to retrieve properties of volcanic plumes. It can be described in three main stages:

– A pixel can be classified as volcanic aerosol using a detection threshold ΔT_{th}, based on BTD between 11 µm and 12 µm, as mentioned in Sect. 3.1 (see Fig. 2). In this study, only pixels with BTD less than ΔT_{th} are considered for the inversions, with ΔT_{th} fixed to −0.5 K to ensure the detection. This threshold depends on the sensor and it would be necessary to precise ΔT_{th} for operational applications. This threshold allows efficiently discriminating volcanic plumes from clouds; however,

AMTD
6, 2793–2828, 2013

some pixels in the plumes with large particle sizes or composed of a mixture of aerosol and cloud particles can be rejected.

- A set of brightness temperatures is simulated with the FASDOM code, for each considered infrared channel, to cover a realistic range of plume optical thickness [0–10] and effective particle radius [0.5–20 µm]. This set is calculated using the LUTs of single scattering properties presented in the previous section and the thermodynamic profile of the atmosphere obtained from the RAMS model (see below for details) for the considered pixel. In addition, the altitude and the temperature of the ash cloud can be estimated from the RAMS model or CALIOP data, if available.

- From a pair of brightness temperatures observed by a sensor in two channels for the considered pixel, retrievals are obtained through linear interpolations from the previous set of simulated brightness temperatures. Especially, a couple of (BTD ; BT at 12 µm) corresponds to a solution of optical thickness and effective size (see Fig. 2). For a given pixel, a solution is sought separately for every particle type presented in Table 1 and several solutions are then possible.

Finally, for each selected pixel, the retrieved parameters are the ash optical thickness at 12 µm, τ_a, and the effective radius of particles, r_e. In addition, mass loading, M (g m^{-2}), which is an important parameter for aviation security, can be easily evaluated from the retrieved effective size and optical thickness as

$$M = \frac{4}{3}\pi\rho r_e^3 \frac{\tau_{12mc}}{k_e L}, \quad (3)$$

with ρ (kg m^{-3}) the density of ash particles, k_e (m) the extinction coefficient and L (m) the geometrical thickness of the ash plume. Note that it is also possible to calculate the mass loading assuming that the size distribution is uniform (i.e., $n(r) = 1$) as

$$M = \frac{4}{3}\rho r_0 \frac{\tau_{12mc}}{Q_e}, \quad (4)$$

AMTD
6, 2793–2828, 2013

with r_0 the geometrical radius and Q_e the extinction cross section.

In complement, we use results of simulations from the 3-D meso-scale model RAMS (Regional Atmospheric Modeling System, Pielke et al., 1992; Cotton et al., 2003) to obtain required data used as input to the FASDOM code, such as the atmospheric profiles and the state of the volcanic plume. Based on meteorological equations and on a simple tracer emission's law, RAMS provides the spatial and temporal evolution of mass loading, its vertical distribution and its transport's altitude (Minvielle et al., 2004a, b). Meteorological parameters of this model are initialized and nudged with ECMWF reanalyzed (0.5 × 0.5 deg.) data. The configuration of simulations consists of one grid (10 × 10 km as spatial resolution) for the studied area, with a vertical discretization of the atmosphere on 50 levels, including 20 levels below 10 km. Simulations are made during a period of several days in order to get the spin-up. The principal event simulated corresponds to the interesting case holding for different satellite observation of 6 May. In particular, for the eruption in 6 May, the volcano source emitted ash over several levels reaching 5 km as observed by P. Arason et al. (2011). Figure 4 presents the spatial distribution of mass loading (vertically integrated) of ash plume on the 6 May. Similarly to the observed one (Fig. 3), the simulated plume get comma pattern due to the NE wind direction over Atlantic Ocean, not so far from volcano source. Simulations are generally in agreement with observation, even if the simulated plume shape appears not so thin as one observed by satellite.

4 Volcanic plume observation

In order to test the sensitivity of retrievals to volcanic particle properties, the algorithm presented in the previous section has been applied in this section to the volcanic plume during the Eyjafjallajökull eruption on 6 May 2010 at 19:00 UTC, using BTD of SEVIRI channels at 11 µm and 12 µm. Retrievals are obtained assuming a lognormal formulation for the size distribution and mass loading is then obtained from Eq. (3). Optical and physical properties are derived assuming an altitude of 6 km for the plume. Indeed, it

AMTD
6, 2793–2828, 2013

has mainly been observed at 5.5–6.5 km height according to IMO's weather radar and it has reached above 9 km level (Hjaltadóttir et al., 2010).

The retrievals of the optical thickness τ_a at 12 µm, of the particle effective radius r_e (µm) and of the mass loading M (g m^{-2}) are presented in Fig. 5. As mentioned in Sect. 3.2, the retrieval algorithm is applied to a given pixel for every particle type reported in Table 1 and several solutions are then possible for r_e and M for the considered pixel. Results presented in Fig. 5 are the mean values of these parameters and they are quite similar to those obtained by Francis et al. (2012) for the same scene, but using only andesite refractive index data (Pollack et al., 1973). In our study, mass loading and effective radius of particles are generally of order of 1–4 g m^{-2} and 2–5 µm, respectively; higher values are observed near the source and can reach 10 g.m^{-2} and 8 µm, respectively. This maximum mass loading is slightly higher than those retrieved by Francis et al. (2012) of about 8 g m^{-2}. The methodology and particle types used in this study can explain this difference. Indeed, the retrieval algorithm employed by Francis et al. (2012) is based on a one-dimensional variational analysis, using andesite refractive indices. The altitude of the plume is then simultaneously retrieved with other physical parameters and not fixed as in our algorithm. The altitude retrieved by Francis et al. (2012) ranges from 3 to 12 km, with most of pixels between 5 and 10 km. This point is detailed in Sect. 6.

In addition, by considering all solutions obtained for the plume in Fig. 5, the retrieved particle type distribution is andesite 8 %, ash 1 %, basalt 7 %, quartz 41 %, hematite 22 %, obsidian 21 %, with a mean effective particle size of $r_e = 4.5\,\mu m \pm 0.8\,\mu m$. The r_e uncertainty is defined as the average of mean deviations obtained for each pixel due to multiple solutions. This uncertainty shows a large dispersion in retrieved effective size by applying the algorithm with several particle types. In addition, less than 5 % of pixels classified as volcanic plume correspond to a unique solution in terms of particle type. At this stage, it seems difficult to retrieve the particle type from only two SEVIRI channels.

AMTD
6, 2793–2828, 2013

In complement, physical parameters of the volcanic plume have been retrieved for the same situation as in Fig. 5, but assuming that the size distribution is uniform (i.e., $n(r) = 1$). The mass loading is then calculated using Eq. (4). In this case, Fig. 6 shows that τ_a and M are very close to those obtained assuming a lognormal formulation for the size distribution. These retrievals are also consistent with those obtained by Prata and Prata (2012) in the same conditions. The lognormal formulation, which is usually used for aerosol studies, has then been used in the following sections.

Previous results have shown that multiple solutions occur when using several particle types. Inversions have then been performed to test the potential of the channel at 8.7 µm to better constrain retrievals. First, Fig. 7a presents retrievals using BTD from SEVIRI channels at 8.7 µm and 12 µm, with similar spatial distributions as in Fig. 5 using the pairs of channels (11 µm; 12 µm). Figure 7a shows that the channel at 8.7 µm can be used for retrievals, but it leads to lower values for retrieved mass loading and effective size, with a mean value of $r_e = 4.0\,\mu m \pm 0.5\,\mu m$. It can be explained by the distribution of retrieved particle type that is slightly different in this case than for simulations presented in Fig. 5, which once again shows that it is difficult to retrieve the plume mineral composition. In a next step, the three channels have been used for retrievals, by only considering pixels for which a solution can be found simultaneously for the two pairs of channels (11 µm; 12 µm) and (8.7 µm; 12 µm). The results that are presented in Fig. 7b appear quite similar to those shown in Fig. 7a, but with a limited number of pixels. However, we can note that the constraint brought by a third channel results in the elimination of the largest sizes. At last, Fig. 8 presents the same results as in Fig. 7b but only for the pixels for which (i) only one particle type is retrieved and (ii) a relative difference less than 20 % is obtained between the effective sizes retrieved with each pairs of channels. This figure shows consistent retrievals but for a very small number of pixels, with mainly three particle types: Hematite 35 %, Obsidian 33 % and Quartz 32 %. In this case, the mean effective radius is about 3.69 µm ± 0.05 µm.

These results show that retrievals are possible using the channel at 8.7 µm but the use of three channels does not allow retrieving the particle composition. It is mainly

AMTD
6, 2793–2828, 2013

due to the spectral characteristics of usual wide field-of-view sensors, with too large spectral band to discriminate the particle type (this point is illustrated in Sect. 6). In addition, the spectral range around 8.7 µm is subject to the ν_1 absorption band of SO_2, which despite weak absolute intensity may appear in high concentration during volcanic eruption. However, low levels of SO_2 have been generally observed during the Eyjafjallajökull eruptions. In addition, analysis has revealed the complex composition of the volcanic plume. As an example, in situ measurements for the Eyjafjallajökull eruption have shown that ash is composed with aggregates of various typologies (Bonadonna et al., 2011). Samples of volcanic ash collected near the source have shown a silica concentration of 58 % (Sigmarsson et al., 2010), suggesting fine to very fine andesite ash (Zehner et al., 2010). This composition can also vary as a function of time and eruptions (Clarisse et al., 2010a). It makes more difficult to retrieve the plume composition using only two or three narrowband channels.

5 Intercomparison of instruments

The algorithm presented in Sect. 3 has been similarly applied to brightness temperature measured by MODIS, SEVIRI and IASI instruments, following the same approach as in Sect. 4. Due to orbits characteristics of satellites, it is possible to compare near-simultaneously retrievals from MODIS and SEVIRI. For the IASI sensor, physical parameters have been retrieved from orbits corresponding to the morning. This intercomparison allows analysing retrievals from instruments with different spatial resolutions and with slightly different spectral configurations.

Figure 9 present retrievals for the plume on 6 May using BTD for MODIS and SEVIRI at 13:45 UTC, and for IASI at 09:50 UTC, with channels at 11 µm and 12 µm. In general, the retrievals show similar patterns for the three instruments. Note that the spatial distribution of retrievals is quite similar to those obtained from the RAMS model (Fig. 4). However, retrievals for the optical thickness, the effective size and the mass loading are slightly higher with MODIS data. The mean effective radius retrieved is about 5.9 µm,

AMTD
6, 2793–2828, 2013

4.35 µm and 5.4 µm for MODIS, SEVIRI and IASI, respectively. The mean retrieved sizes should be explained by the spectral characteristics of instruments. As an example, the central wavelengths of MODIS channel are closer to those selected for IASI. Table 2 presents the distribution of particle type and corresponding mean effective radius retrieved as a function of the instrument. Retrievals are quite similar using MODIS and IASI, but different using SEVIRI data for the same scene. Consequently, it seems difficult to retrieve the particle composition from narrow band sensors, as already mentioned in Sect. 4. Note that the time lag between observations may also partially explain differences in retrievals.

In addition, Fig. 9 shows that the mass loading decreases with the spatial resolution of the instrument. Indeed, higher values are retrieved from MODIS compare to SEVIRI and IASI, with maximal up to 10 g m^{-2}. It is likely due to the coarser spatial resolution of the instruments. The influence of the spatial resolution on retrievals has been also illustrated from simulations with MODIS and IASI data. The bottom panel of Fig. 9 presents retrievals of physical parameters estimated from MODIS data averaged over the same IFOV than IASI. It shows similar spatial distribution of the effective size and mass loading obtained from available IASI data or averaged brightness temperatures from MODIS. These results confirm the influence of the spatial resolution on volcanic plume retrievals and that algorithms using infrared measurements provide consistent retrievals for physical parameters, although differences in spatial resolution.

Note that comparisons have also been performed between SEVIRI and IASI using measurements acquired in the afternoon of 6 May and they have also shown consistency of retrievals (not presented here). In the same manner, comparisons are also possible with the three-channel Imaging Infrared Radiometer (IIR) onboard CALIPSO (Garnier et al., 2012; Sourdeval et al., 2012). Indeed, IIR performs measurements nearly simultaneously with observations of MODIS at a similar spatial resolution. Nevertheless, because the IIR instrument has a very narrow measurement swath, spatio-temporal collocations between IIR and volcanic plume are not frequent. However, retrievals have been obtained using IIR data for the same situation as for MODIS and

AMTD
6, 2793–2828, 2013

SEVIRI. Similar results have been obtained, but only a very few pixels are available for comparisons (not presented here).

6 Retrieval uncertainties

Previous comparisons have revealed a satisfactory level of agreement between retrievals of several sensors despite their different spatial and spectral characteristics. However, Sect. 4 has also shown that parameters such as plume altitude or particle type can have an important influence on retrievals. Uncertainties due to these parameters are analysed in this section.

6.1 Effect of plume height

In the same manner, the impact of the plume altitude on the retrieved parameters has been evaluated. Figure 10 presents retrievals obtained with our algorithm assuming a volcanic plume at 6 km (Fig. 10a) or 8 km height (Fig. 10b), using andesite refractive indices. These results are in general consistent with those of Francis et al. (2012). However, we can note that the altitude has a significant impact on retrievals, especially on the number of detected pixels. Indeed, Fig. 10 shows that our inversion method leads to a larger number of pixels assuming a plume at 8 km height. In addition, effective sizes retrieved with a plume at 8 km height are larger near the source than those retrieved with a lower altitude. The mean effective radius is equal to 3.6 µm and 3.8 µm for a plume at 5 km and 8 km height, respectively. These simulations show that multiple solutions can be found for a given pixel assuming a plume at different altitude and/or with different refractive indices. Consequently, if the general pattern of retrieved physical parameters seems correct at large scale, uncertainties can lead to local discrepancies on the retrieved physical parameters and make difficult an accurate determination of maximal values for the particle size and the total column load of the plume.

AMTD
6, 2793–2828, 2013

6.2 Aerosol type effect

Spatial distribution of the particle effective radius and the mass loading are presented in Fig. 11 by considering only, in one hand, quartz refractive index data or, in the other hand, hematite and obsidian. Indeed, simulations have shown similar retrievals using hematite and obsidian refractive indices. Figure 11 presents noticeable differences in the retrieved parameters r_e and M, with higher values using quartz refractive indices. These results may explain the high maximum values presented in Fig. 5 and discrepancies with estimations presented by Francis et al. (2012). The mean effective radius in Fig. 11 is about 6.3 µm or 3.3 µm using quartz or hematite and obsidian, respectively. The spatial distribution of the optical thickness at 12 µm retrieved in the two cases is, however, similar. Figure 11 shows that uncertainties due to the aerosol type can lead to factor of two on the effective size and mass loading retrievals. As mentioned by Francis et al. (2012), these results confirm that retrievals using BTD from SEVIRI channels at 11 µm and 12 µm are sensitive to the refractive indices, which therefore represents a major source of uncertainties.

Previous intercomparisons have shown that various spectral and spatial resolutions lead to consistent retrievals for the effective size and mass loading. Narrow band sensors represent valuable instruments for temporal monitoring of volcanic plumes or for rough estimates of characteristics such as the mass loading. However, due to their spectral properties, they are not well adapted for an accurate characterisation of the plume composition. In the previous analysis, IASI data have been used in the same configuration than narrow band sensors in order to ensure consistent comparisons. However, IASI has a high spectral resolution that enables a fine characterization of the physical properties of the observed plume (Clarisse et al., 2010a, b). As an example, Fig. 12 presents IASI spectra simulated for a plume, assuming different particle types and effective size, for a fixed optical thickness of 0.5 at 12 µm. Brightness temperatures that would be observed with SEVIRI in the same conditions are also reported. Figure 12 shows that a plume with different particle properties can lead to similar SEVIRI

AMTD
6, 2793–2828, 2013

brightness temperature, which makes it impossible to disentangle between them. By contrast, the simulated spectra for IASI clearly shows different signatures in the 1050–1250 cm^{-1} spectral region and an estimate of plume properties would be possible in this case. As a consequence, the use of hyperspectral sensors, such as IASI, would improve the determination of plume composition, using appropriate numerical methods.

7 Conclusions

A methodology has been presented for retrievals of optical and physical parameters of volcanic ash plumes using thermal infrared remote sensing. It has been applied to infrared instruments commonly used for the monitoring of aerosols, such as SEVIRI, IASI or MODIS. Comparisons have shown the consistency of retrievals of effective size and mass loading using these instruments, despite the differences of spectral or spatial resolution. However, our study also pointed out uncertainties on retrievals from spaceborne narrow band sensors, due to parameters such as the plume height or the particle type. Indeed, multiple solutions can then be found for a given pixel assuming a plume at different altitude and/or composition of particles with different refractive indices. This can lead to large retrieval errors on the effective size and mass loading in the densest areas of volcanic ash clouds. It is due to the large spectral width of narrow band sensors that is not sensitive enough to the particle type. In addition, the use of a third channel at 8.7 µm does not enable to retrieve the aerosol type.

In this context, high spectral resolution measurements can be very useful for a characterisation of the plume composition. Simulations performed in this study using the spectral configuration of IASI have confirmed that infrared sounders have adequate spectral characteristics to derive the plume composition. However, these high spectral resolution data requires the use of appropriate numerical approaches such as optimal estimation methods. As an example, Herbin et al. (2012) have presented such a theoretical approach from multispectral information of the TANSO-FTS instrument that

AMTD
6, 2793–2828, 2013

enables simultaneous retrievals of gases profiles as well as aerosol granulometry and concentration. This methodology would be well-suited for monitoring volcanoes from hyperspectral sensors.

Acknowledgements. This work was supported by the "Centre National d'Etudes Spatiales" (CNES – TOSCA), and the "Programme National de Télédétection Spatiale" (PNTS). The authors thank the ICARE Data and Services Center www.icare.univ-lille1.fr, (for SEVIRI, MODIS and IIR data) and Ether CNES/CNRS-INSU Ether web site http://www.pole-ether.fr, (for IASI data) for providing access to satellite data, and the French national computing centre CINES (Centre Informatique National de l'Enseignement Supérieur) for donation of computational time.

The publication of this article is financed by CNRS-INSU.

References

Arason, P., Petersen, G. N., and Bjornsson, H.: Observations of the altitude of the volcanic plume during the eruption of Eyjafjallajökull, April–May 2010, Earth Syst. Sci. Data, 3, 9–17, doi:10.5194/essd-3-9-2011, 2011.

Bonadonna, C., Genco, R., Gouhier, M., Pistolesi, M., Cioni, R., Alfano, F., Hoskuldsson, A., and Ripepe, M.: Tephra sedimentation during the 2010 Eyjafjallajökull eruption (Iceland) from deposit, radar, and satellite observations, J. Geophys. Res., 116, B12202, doi:10.1029/2011JB008462, 2011.

Borde, R. and Dubuisson, P. : Sensitivity of Atmospheric Motion Vectors Height Assignment methods to semi-transparent cloud properties using simulated Meteosat-8 radiances, J. Appl. Meteorol. Clim., 49, 1191–1204, 2010.

AMTD
6, 2793–2828, 2013

Clarisse, L., Prata, F., Lacour, J.-L., Hurtmans, D., Clerbaux, C., and Coheur, P.-F.: A correlation method for volcanic ash detection using hyperspectral infrared measurements, Geophys. Res. Lett., 37, L19806, doi:10.1029/2010GL044828, 2010a.

Clarisse, L., Hurtmans, D., Prata, A. J., Karagulian, F., Clerbaux, C., De Mazière, M., and Coheur, P.-F.: Retrieving radius, concentration, optical depth, and mass of different types of aerosols from high-resolution infrared nadir spectra, Appl. Optics, 49, 3713–3722, 2010b.

Clerbaux, C., Boynard, A., Clarisse, L., George, M., Hadji-Lazaro, J., Herbin, H., Hurtmans, D., Pommier, M., Razavi, A., Turquety, S., Wespes, C., and Coheur, P.-F.: Monitoring of atmospheric composition using the thermal infrared IASI/MetOp sounder, Atmos. Chem. Phys., 9, 6041–6054, doi:10.5194/acp-9-6041-2009, 2009.

Cotton, W. R., Pielke, R. A., Walko, R. L., Liston, G. E., Tremback, C. J., Hiang, H., McAnelly, R. L., Harrington, J. Y., Nicholls, M. E., Carrio, G. G., and McFadden, J. P.: RAMS 2001: Current status and future directions, Meteorol. Atmos. Phys., 82, 5–29, 2003.

Dubovik, O., Holben, B., Eck, T. F., Smirnov, A., Kaufman, Y. J., King, M. D., Tanré, D., and Slutsker, I.: Variability of absorption and optical properties of key aerosol types observed in worldwide locations, J. Atmos. Sci., 59, 590–608, 2002.

Dubuisson, P., Giraud, V., Chomette, O., Chepfer, H., and Pelon, J.: Fast radiative transfer modeling for infrared imaging radiometry, J. Quant. Spectrosc. Ra., 95, 201–220, 2005.

Dubuisson, P., Giraud, V., Pelon, J., Cadet, B., and Yang, P.: Sensitivity of thermal infrared radiation at the top of the atmosphere and the surface to ice cloud microphysics, J. Appl. Meteor. Clim., 47, 2545–2560, doi:10.1175/2008JAMC1805.1, 2008.

Francis, P. N., Cooke, M. C., and Saunders, R.: Retrieval of physical properties of volcanic ash using Meteosat: A case study from the 2010 Eyjafjallajökull eruption, J. Geophys. Res., 117, D00U09, doi:10.1029/2011JD016788, 2012.

Garnier, A., Pelon, J., Dubuisson, P., Faivre, M., Chomette, O., Pascal, N., and Kratz, D. P.: Retrieval of Cloud Properties Using CALIPSO Imaging Infrared Radiometer. Part I: Effective Emissivity and Optical Depth, J. Appl. Meteor. Clim., 51, 1407–1425, doi:10.1175/JAMC-D-11-0220.1, 2012.

Herbin, H., Labonnote, L. C., and Dubuisson, P.: Multispectral information for gas and aerosol retrieval from TANSO-FTS instrument, Atmos. Meas. Tech. Discuss., 5, 8435–8468, doi:10.5194/amtd-5-8435-2012, 2012.

Hess, M., Koepke, P., and Schult, I.: Optical Properties of Aerosols and Clouds: The Software Package OPAC, B. Am. Meteorol. Soc., 79, 831–844, 1998.

AMTD
6, 2793–2828, 2013

Hjaltadóttir, S., Sigmundsson, F., Oddsson, B., Hreinsdóttir, S., Roberts, M. J., and Sveinbjörnsson, H.: Eruption in Eyjafjallajökull Status report: 18:00 GMT, 6 May 2010, Icelandic Meteorological Office and Institute of Earth Sciences, University of Iceland, 2010.

Inoue, T.: On the temperature and effective emissivity determination of semi-transparent cirrus clouds by bi-spectral measurements in the window region, J. Meteorol. Soc. Jpn., 63, 88–98, 1985.

Inoue, T.: A cloud type classification with NOAA 7 split-window measurements, J. Geophys. Res., 92, 3991–4000, 1987.

Kratz, D. P.: The correlated k-distribution technique as applied to the AVHRR channels, J. Quant. Spectrosc. Ra. Transfer, 53, 501–517, 1995.

Kuze, A., Suto, H., Nakajima, M., and Hamazaki, T.: Thermal and near infrared sensor for carbon observation Fourier-transform spectrometer on the Greenhouse Gases Observing Satellite for greenhouse gases monitoring, Appl. Optics, 48, 6716–6733, 2009.

Lacis, A. A. and Oinas, V.: A Description of the correlated k-distribution method, J. Geophys. Res., 96, 9027–9064, 1991.

Le Treut, H., Somerville, R., Cubasch, U., Ding, Y., Mauritzen, C., Mokssit, A., Peterson, T., and Prather, M.: Historical Overview of Climate Change, in: Climate Change 2007: The Physical Science Basis. Contribution of Working Group I to the Fourth Assessment Report of the Intergovernmental Panel on Climate Change, edited by: Solomon, S., Qin, D., Manning, M., Chen, Z., Marquis, M., Averyt, K. B., Tignor M., and Miller, H. L., Cambridge University Press, Cambridge, United Kingdom and New York, NY, USA, 2007.

Longtin, D. R., Shettle, E. P., Hummel, J. R., and Pryce, J. D.: A Wind Dependent Desert Aerosol Model: Radiative Properties, AFGL-TR-88- 0112, Air Force Geophysics Laboratory, Hanscom AFB, MA, 1988.

Mehta, P., Harries, J. E., and Turner, D. D.: Effect of size distribution and particle shape on simulations of downwelling infrared spectra during Saharan dust storms, Current problems in atmospheric radiation, Proceedings of the International Radiation Symposium (IRS), Foz do Iguacu, Brazil, 3–8 August 2008, AIP Conf. Proc., 1100, 177–180, doi:10.1063/1.3116943, 2008.

Minvielle, F., Cautenet, G., Lasserre, F., Forêt, G., Cautenet, S., Léon, J.-F., Andreae, M. O., Mayol-Bracero, O. L., Gabriel, R., Chazette, P., and Roca, R.: Modeling of the transport of aerosols during INDOEX 1999 and comparison with experimental data, Part 1: carbonaceous aerosol distribution, Atmos. Environ., 38, 1811–1822, 2004a.

AMTD
6, 2793–2828, 2013

Minvielle, F., Cautenet, G., Lasserre, F., Forêt, G., Cautenet, S., Léon, J.-F., Andreae, M. O., Mayol-Bracero, O. L., Gabriel, R., Chazette, P., and Roca, R.: Modeling the transport of aerosols during INDOEX 1999 and comparison with experimental data. Part 2: continental aerosol and their optical depth, Atmos. Environ., 38, 1823–1837, 2004b.

Pielke, R. A., Cotton, W. R., Walko, R. L, Tremback, C. J., Lyons, W. A., Grasso, L. D., Nicholls, M. E., Moran, M. D., Wesley, D. A., Leel, T. J., and Copeland, J. H.: A comprehensive meteorological modeling system RAMS, Meteorol. Atmos. Phys., 49, 69–91, 1992.

Pollack, J. B., Toon, O. B., and Khare, B. N.: Optical properties of some terrestrial rocks and glasses, Icarus, 19, 372–389, 1973.

Prata, A. J.: Infrared radiative transfer calculations for volcanic ash clouds, Geophys. Res. Lett., 16, 1293–1296, doi:10.1029/GL016i011p01293, 1989a.

Prata, A. J.: Observation of volcanic ash clouds using AVHRR-2 radiances, Int. J. Remote Sens., 10, 751–761, doi:10.1080/01431168908903916, 1989b.

Prata, A. J. and Grant, I. F.: Retrieval of microphysical and morphological properties of volcanic ash plumes from satellite data: Application to Mt. Ruapehu, New Zealand., Q. J. Roy. Meteorol. Soc., 127, 2153–2179, 2001.

Prata, A. J. and Kerkmann, J.: Simultaneous retrieval of volcanic ash and SO_2 using MSG-SEVIRI measurements, Geophys. Res. Lett., 34, L05813, doi:10.1029/2006GL028691, 2007.

Prata, A. J. and Tupper, A. T.: Aviation hazards from volcanoes: the state of the science, Nat. Hazards, 51, 239–244, doi:10.1007/s11069-009-9415-y, 2009.

Prata, F. J. and Prata, A. T.: Eyjafjallajokull volcanic ash concentrations determined using SEVIRI measurements, *J. Geophys. Res.*, doi:10.1029/2011JD016800, 2012.

Remer, L. A., Kaufman, Y. J., Tanré, D., Mattoo, S., Chu, D. A., Martins, J. V., Li, R.-R., Ichoku, C., Levy, R. C., Kleidman, R. G., Eck, T. F., Vermote, E., and Holben, B. N.: The MODIS aerosol algorithm, products and validation, J. Atmos. Sci., 62, 947–973, 2005.

Schlüssel, P., Hultberg, T. H., Phillips, P. L., August, T., and Calbet, X.: The operational IASI Level 2 processor, Adv. Space Res., 36, 982–988, 2005.

Schneider, D. J., Rose, W. I., and Kelley, L.: Tracking of 1992 eruption clouds from Crater Peak vent of Mount Spurr Volcano, Alaska, using AVHRR, edited by: Keith, T. E. C., The 1992 eruptions of Crater Peak vent, Mount Spurr Volcano, Alaska, US Geological Survey Bulletin B 2139, 27–36, 1995.

AMTD
6, 2793–2828, 2013

Schmetz, J., Mhita, M., and van den Berg, L.: METEOSAT Observations of Longwave Cloud-Radiative Forcing for April 1985, J. Climate, 3, 784–791, 1990.
Shettle, E. P. and Fenn, R. W.: Models for the aerosols of the lower atmosphere and the effects of humidity variations on their optical properties, AFGL-TR-79-0214, 1979.
Sigmarsson, O., Óskarsson, N., Þórðarson, P., Larsen, G., and Höskuldsson, A.: Preliminary interpretations of chemical analysis of tephra from Eyjafjallajökull volcano, Institute of Earth Sciences – Nordic Volcanological Institute, 2 pp., 2010.
Sourdeval, O., Brogniez, G., Pelon, J., Labonnote, C.-L., Dubuisson, P., Parol, F., Josset, D., Garnier, A., Faivre, M., and Minikin, A.: Validation of IIR/CALIPSO Level 1 Measurements by Comparison with Collocated Airborne Observations during CIRCLE-2 and Biscay '08 Campaigns, J. Atmos. Ocean. Tech., 29, 653–667, doi:10.1175/JTECH-D-11-00143.1, 2012.
Stamnes, K., Tsay, S., Wiscombe, W., and Jayaweera, K.: Numerically stable algorithm for discrete-ordinate-method radiative transfer in multiple scattering and emitting layered media, Appl. Optics, 27, 2502–2509, 1988.
Wen, S. and Rose, W. I.: Retrieval of sizes and total masses of particles in volcanic clouds using AVHRR channels 4 and 5, J. Geophys. Res., 99, 5421–5431, 1994.
Winker, D. M., Liu, Z., Omar, A., Tackett, J., and Fairlie, D.: CALIOP observations of the transport of ash from the Eyjafjallajökull volcano in April 2010, J. Geophys. Res., 117, D00U15, doi:10.1029/2011JD016499, 2012.
Zehner, C. (Ed.): Monitoring Volcanic Ash from Space, Proceedings of the ESA-EUMETSAT workshop on the 14 April to 23 May 2010 eruption at the Eyjafjoll volcano, South Iceland. Frascati, Italy, 26–27 May 2010, ESA-Publication STM-280, doi:10.5270/atmch-10-01, 2010.

AMTD
6, 2793–2828, 2013

Table 1. Density D of particle types and references used in this study.

Particle type	D (g cm^{-3})	T (K)	Ref.
Andesite	2.65		1
Volcanic Ash	2.8	293	2
Basalt	2.9		1
Hematite	5.1	293	3
Obsidian	2.65		1
Quartz	2.65	293	3

Ref.: 1 – Pollack (1973); 2 – Shettle and Fenn (1979); 3 – Longtin et al. (1988).

AMTD
6, 2793–2828, 2013

Table 2. Percentage (%) of particle type and effective radius r_e retrieved for the plume on 6 May (see Fig. 9) as a function of the sensor.

	MODIS		SEVIRI		IASI	
Particle type	%	r_e (µm)	%	r_e (µm)	%	r_e (µm)
Andesite	18	6.4	14	3.3	18	6.3
Volcanic Ash	21	4.6	2	4.7	13	5.3
Basalt	18	5.6	11	3.2	18	5.6
Hematite	21	6.5	18	3.9	20	5.1
Obsidian	17	6.3	21	3.3	18	4.5
Quartz	5	7.6	34	6.0	12	6.2

AMTD
6, 2793–2828, 2013

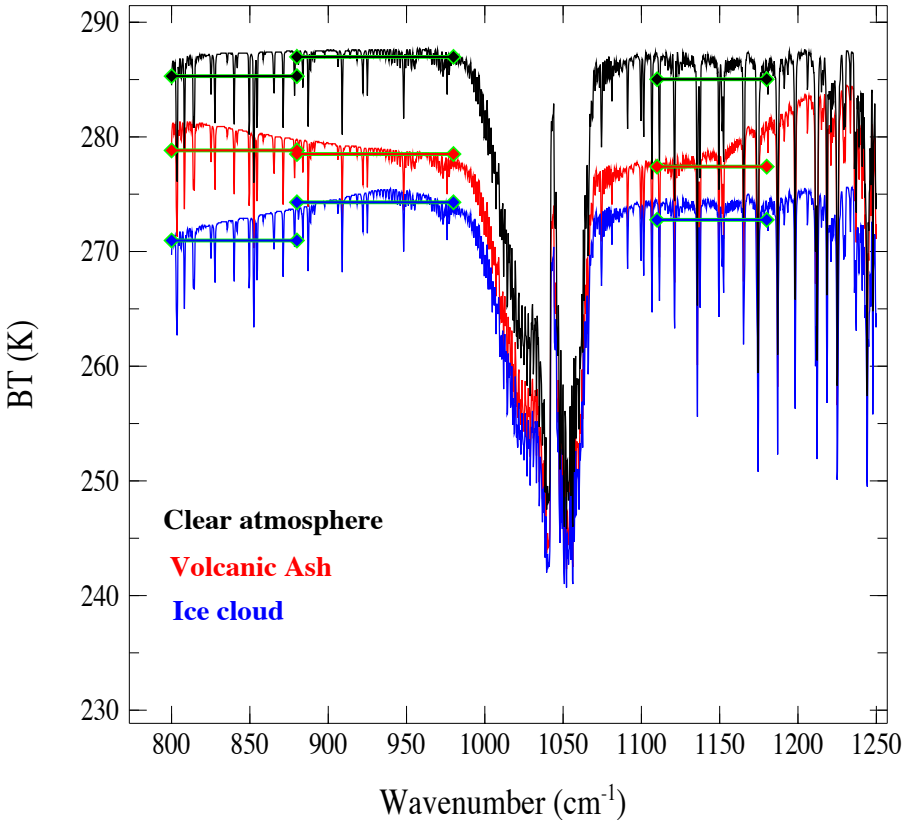

Fig. 1. IASI spectra simulated with the LBLDOM code, assuming a clear gaseous atmosphere (black), an ice cloud at 10 km height with an optical thickness of 0.4 at 12 µm and particle size of 10 µm (blue), a volcanic ash plume at 6 km height with an optical thickness of 0.2 at 12 µm and particle effective size of 2 µm (red). Horizontal bars represent SEVIRI simulations for the channels at 8.7, 10.8 and 12 µm (1150, 910 and 833 cm^{-1}, respectively), with the spectral width associated to each channel.

AMTD
6, 2793–2828, 2013

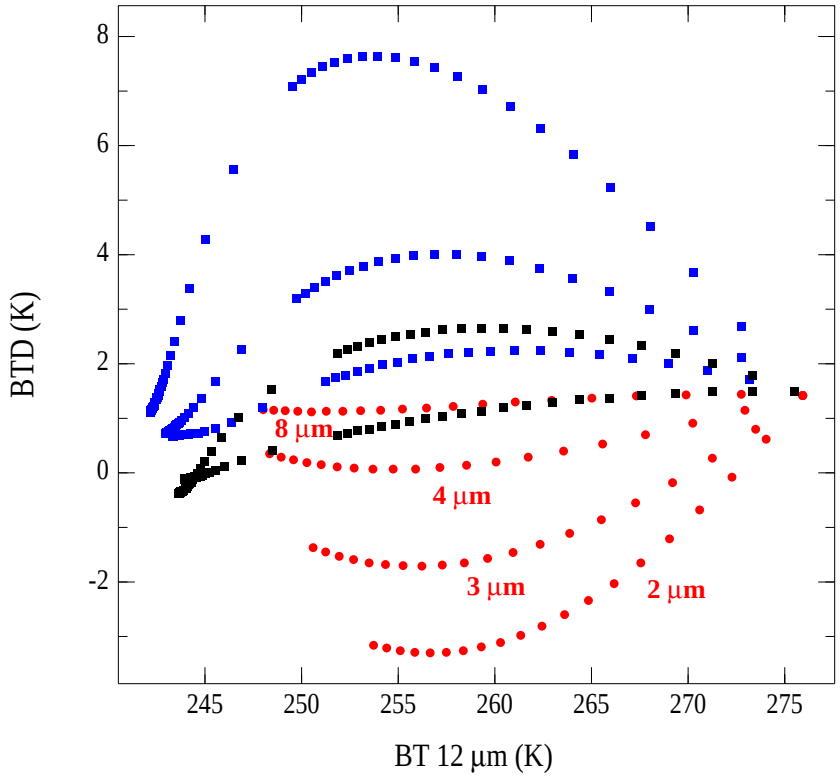

Fig. 2. Brightness Temperature Differences (BTD), from SEVIRI channels at 10.8 µm and 12 µm, as a function of Brightness Temperature (BT) at 12 µm, simulated with the FASDOM radiative transfer code. BTD are reported in red for a volcanic plume at 6 km height with andesite particles for different effective size (2 to 8 µm) and a plume optical thickness at 12 µm ranging from 0 to 1. Typical signature of ice cloud (blue) and liquid cloud (black) are also reported for effective radius ranging from 4 to 20 µm and a cloud optical thickness at 12 µm ranging from 0 to 50.

AMTD
6, 2793–2828, 2013

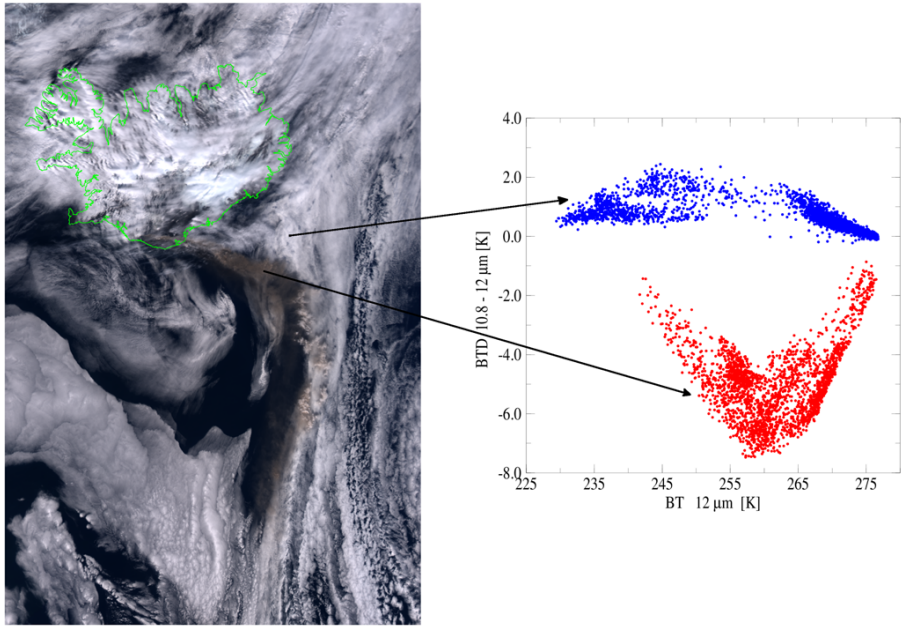

Fig. 3. Example of Brightness Temperature Differences (BTD) observed for the Eyjafjallajökull volcanic plume using AQUA/MODIS data. The RGB composite image is presented on 6 May 2010 (left). BTD (11–12 µm) are reported as a function of Brightness Temperature (BT) at 12 µm (right), in the volcanic plume (red) or a cloudy area (blue).

AMTD
6, 2793–2828, 2013

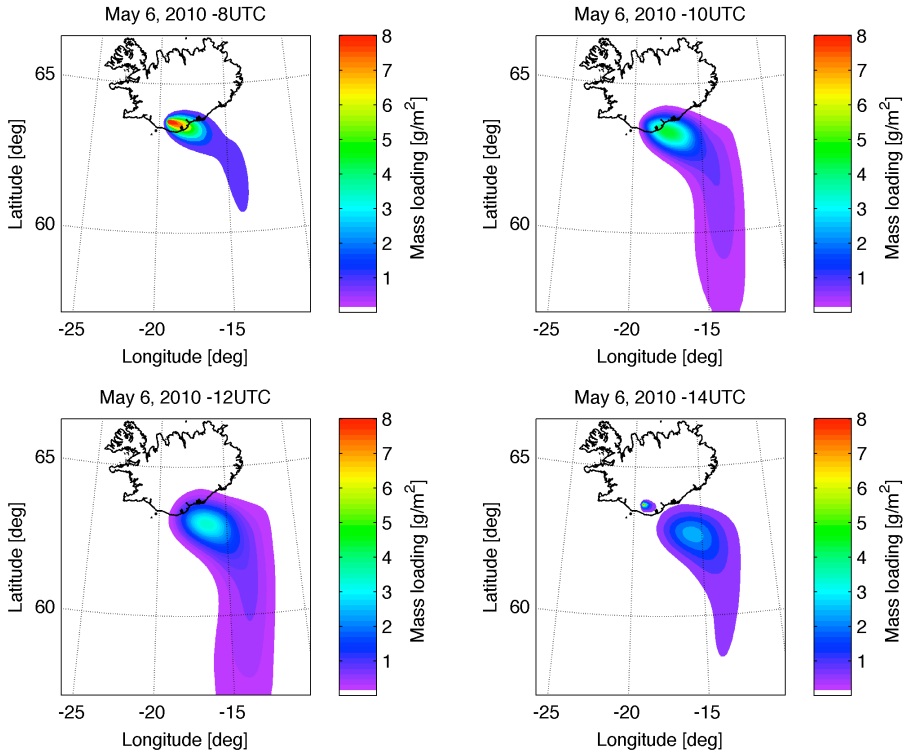

Fig. 4. Temporal and spatial evolution of mass loading obtained by RAMS model on 6 May, from 08:00 to 14:00 UTC.

AMTD
6, 2793–2828, 2013

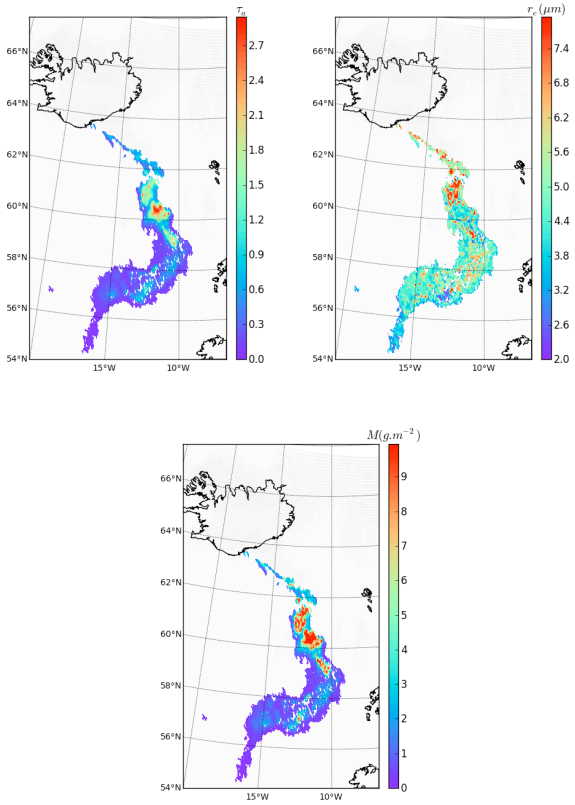

Fig. 5. Optical thickness at 12 µm τ_a, effective radius r_e and mass loading M retrieved using SEVIRI data on 6 May 2010 at 19:00 UTC. Retrievals are defined as mean values obtained from several particle models (see Sect. 4 for details), assuming a lognormal formulation for the size distribution and using BTD from SEVIRI channels at 10.8 µm and 12 µm.

AMTD
6, 2793–2828, 2013

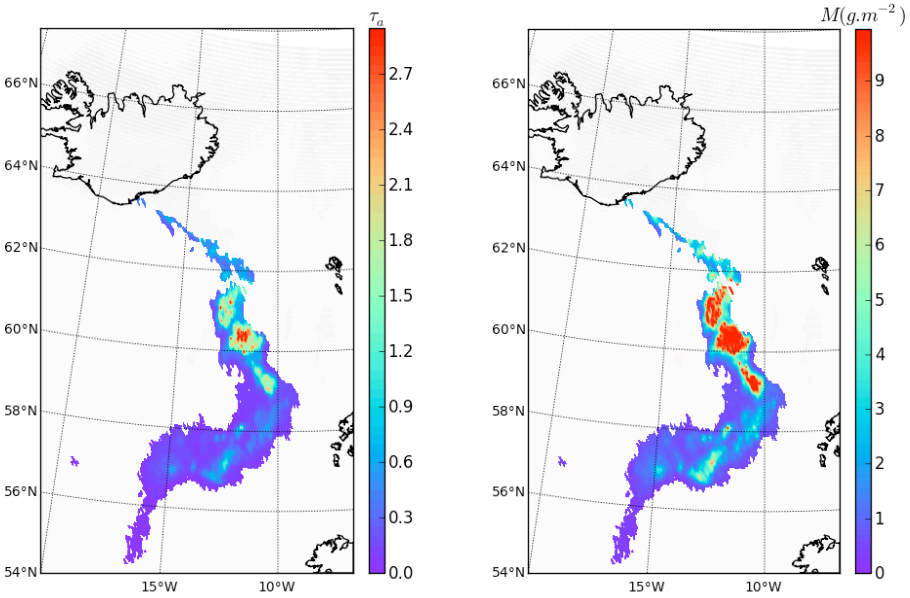

Fig. 6. Similar as Fig. 5 for the effective radius r_e and the mass loading M, but assuming that the size distribution is uniform (i.e., $n(r) = 1$).

AMTD
6, 2793–2828, 2013

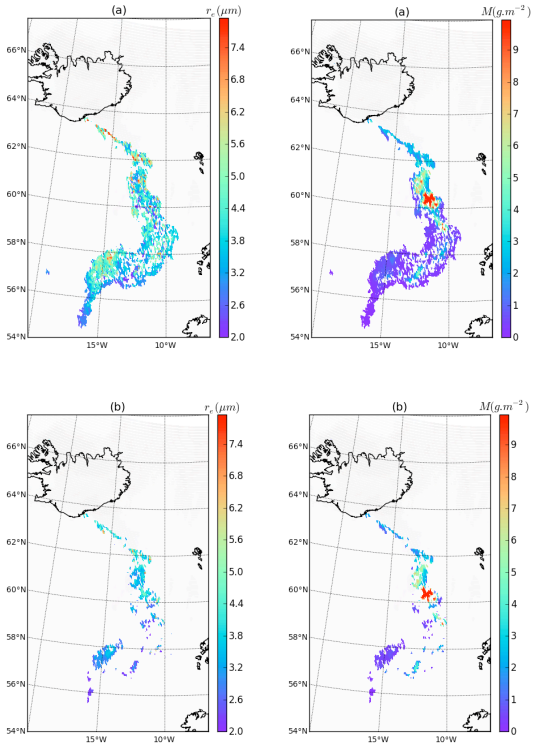

Fig. 7. Similar as Fig. 5, but **(a)** using BTD from two SEVIRI channels at 8.7 µm and 12 µm or **(b)** using the three channels at 8.7 µm, 10.8 µm and 12 µm.

AMTD
6, 2793–2828, 2013

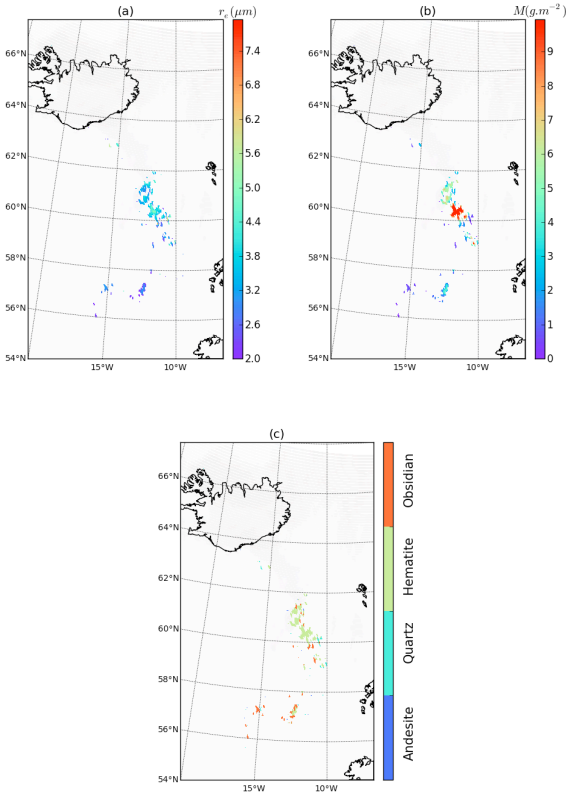

Fig. 8. Similar as Fig. 7b, but for pixels with only one retrieved particle type **(a)** and **(b)**. **(c)** presents the retrieved spatial distribution for the retrieved particle type.

AMTD
6, 2793–2828, 2013

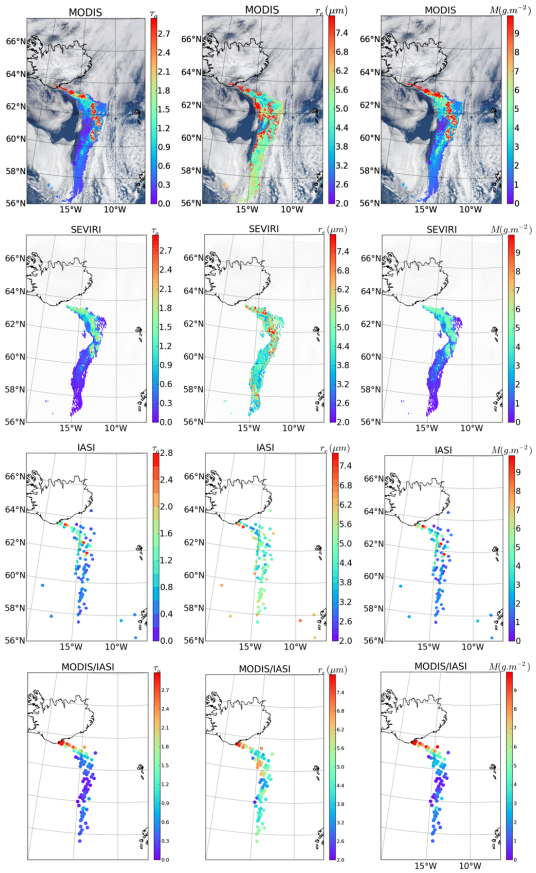

Fig. 9. Retrievals of optical thickness τ_a at 12 µm (left column), effective radius r_e (middle column) and mass loading M (right column) on 6 May, using MODIS, SEVIRI, IASI instruments. The bottom figures (MODIS/IASI) present retrievals using MODIS data as seen by IASI.

AMTD
6, 2793–2828, 2013

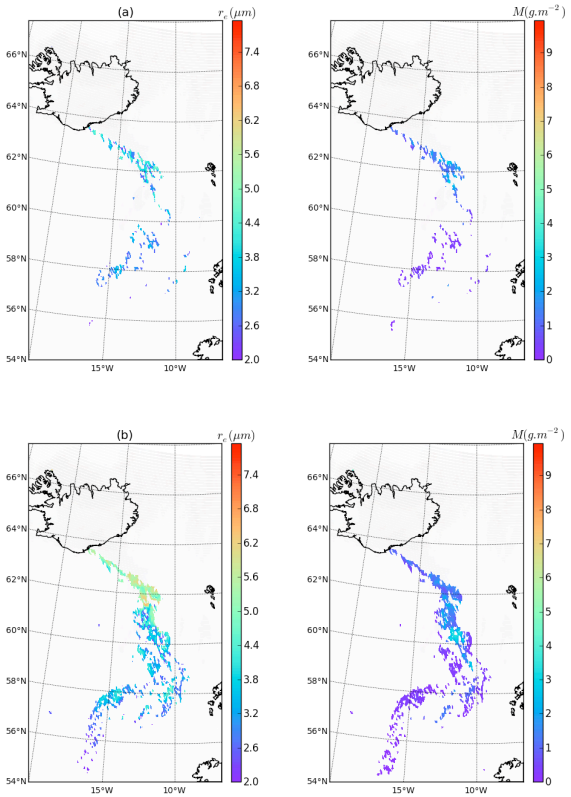

Fig. 10. Effective radius r_e (left) and mass loading M (right) retrieved using SEVIRI data on 6 May 2010 at 19:00 UTC, as in Fig. 5 but assuming only andesite refractive index and with volcanic plume **(a)** at 6 km height (top figures) or **(b)** at 8 km height (bottom figures).

AMTD
6, 2793–2828, 2013

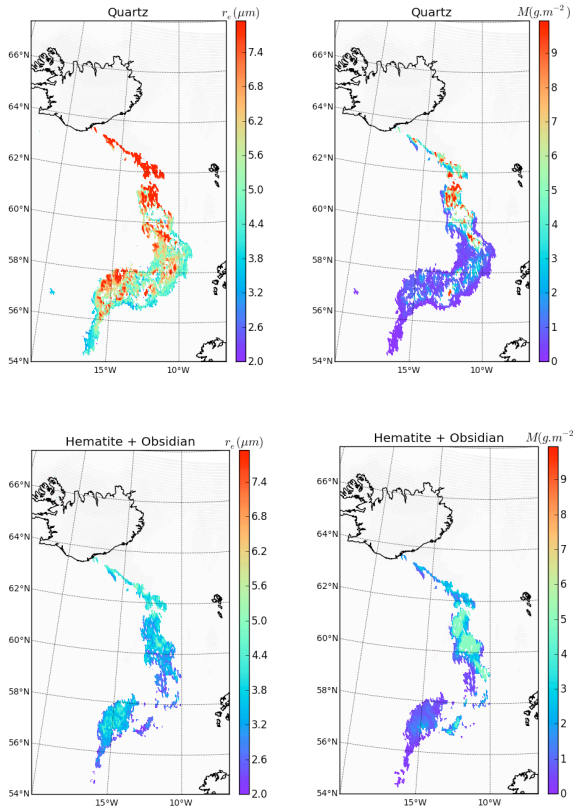

Fig. 11. Effective radius r_e (left) and mass loading M (right) retrieved using SEVIRI data on 6 May 2010 at 19:00 UTC, as in Fig. 5 but considering only quartz (top) or hematite and obsidian (bottom) refractive index data.

AMTD
6, 2793–2828, 2013

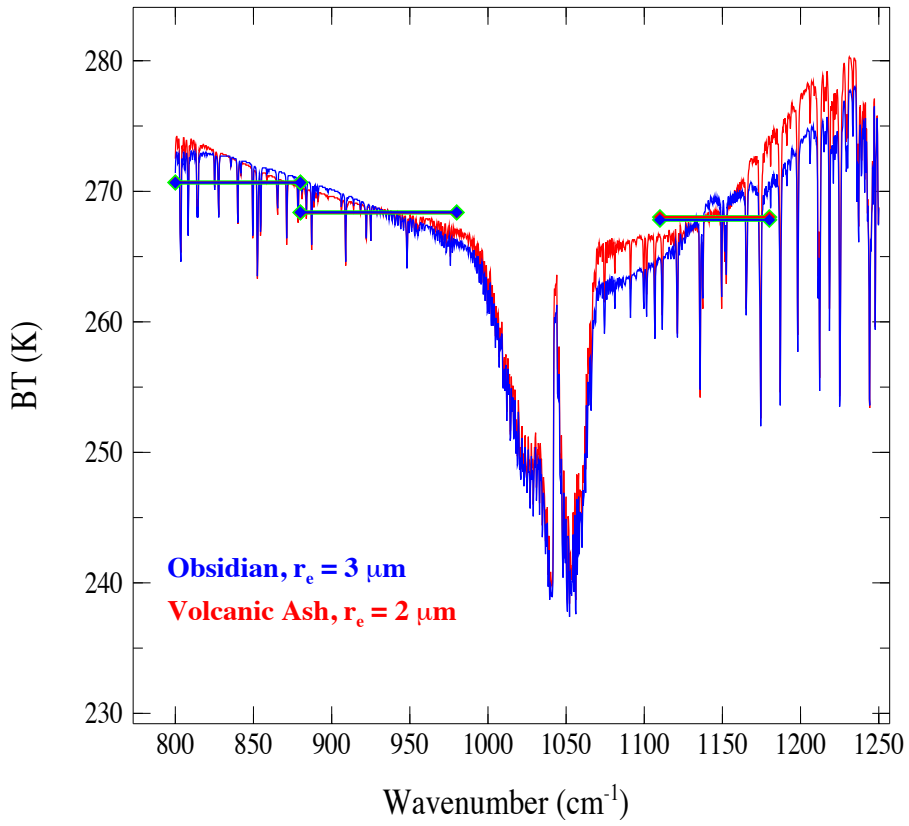

Fig. 12. IASI spectra simulated with the LBLDOM code, assuming a volcanic plume at 6 km height with a fixed optical thickness of 0.5 at 12 µm, for the two following cases: volcanic ash data with particle effective radius r_e of 2 µm (Red) or obsidian data with r_e of 3 µm (blue). Horizontal bars represent SEVIRI simulations corresponding to the two previous cases (with the same colour code), for the channels at 8.7, 10.8 and 12 µm (1150, 910 and 833 cm^{-1}, respectively) and with the spectral width associated to each channel.

AMTD
6, 2793–2828, 2013